molecular pharmaceutics

Brief Article

pubs.acs.org/molecularpharmaceutics

Bioimaging of Intravenous Polymeric Micelles Based on Discrimination of Integral Particles Using an Environment-Responsive Probe

Haisheng He,[†,§] Jian Zhang,[†,‡,§] Yunchang Xie,[†] Yi Lu,[†] Jianping Qi,[†] Ejaj Ahmad,[†] Xiaochun Dong,[†] Weili Zhao,[*,†,‡] and Wei Wu[*,†]

[†]School of Pharmacy, Fudan University, Key Laboratory of Smart Drug Delivery of MOE and PLA, Shanghai 201203, China

[‡]Key Laboratory for Special Functional Materials of the Ministry of Education, Henan University, Kaifeng 475001, China

Supporting Information

ABSTRACT: One of the biggest challenges in bioimaging of nanoparticles is how to identify integral particles from bulk signals of probes. Signals of free probes are always mistakenly counted into total signals of particles. In this study, *in vivo* fate of intravenous polymeric micelles (PMs, $mPEG_{2.5k}$–$PDLLA_{2.5k}$) was explored using a highly sensitive near-infrared environment-responsive fluorescent probe. This probe is able to emit fluorescence when embedded in nanocarriers but quench spontaneously and absolutely upon release into water, based on the aggregation-caused quenching effect, which means that the interference generated by free probes can be completely diminished. Analysis of blood-borne fluorescence reveals rapid clearance of PMs from blood following a tricompartmental pharmacokinetic model. Live imaging shows pervasive distribution of PMs throughout the body, and a tendency of accumulation to extremities with fluorescence density 3–5 times higher than the trunk. *Ex vivo* examination reveals that most PMs are found in vital organs following an order of lung > liver > spleen > heart > kidney in concentration, but an order of liver > lung > spleen > heart ≈ kidney in total amount. The distribution to other organs and tissues is even lower, and to brain, negligible. It is concluded that the biodistribution of PMs to vital organs and extremities warns of potential toxicity and can be translated to explain the toxicity of its commercial counterpart with similar chain lengths.

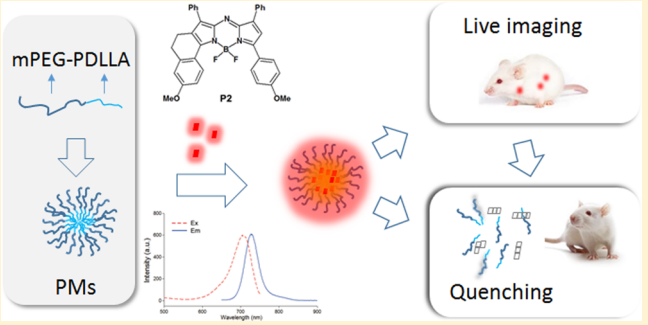

KEYWORDS: *polymeric micelles, PEG–PLA, long-circulating, stealth, bioimaging, biodistribution, environment-responsive, fluorescent probes*

INTRODUCTION

PEGylation of nanovehicles, thereby imparting long-circulating or stealth properties to them, has become a paradigm in the field of targeted drug delivery for cancer therapy.[1,2] Coating with hydrophilic polyethylene glycol (PEG) chains has been employed to camouflage the nanovehicles to evade opsonization by plasma opsonins and divert them to organs outside of the reticulo-endothelial system (RES) with extensively enhanced elimination half-life and accumulation in tumors based on the well-known enhanced permeability and retention (EPR) effect.[3,4] The successful marketing of stealth doxorubicin liposomes (Doxil) represents a landmark in the long march of development of nanoparticulate drug delivery systems.[5,6] Recently, another kind of nanovehicles, polymeric micelles (PMs), draws significant attention in the field of drug delivery,[7−12] and the marketing of paclitaxel PEG-poly(lactic acid) (PLA) PMs with a brand name of Genexol adds another weapon to the long-circulating arsenal.[13,14] However, in contrast to the substantial quantity of publications on this issue, the number of product certificates seems to be negligible. How to bridge the gap remains at the center of heated discussions and investigations.

From both the academics and the industries, translational research is gradually recognized as the bottleneck that impedes the research and development of nanoparticulate drug delivery systems. The understanding of *in vivo* behaviors of nanocarriers represents one of the most essential tasks in translation of basic research into clinical applications or products. Previous knowledge on *in vivo* fate of nanocarriers is generally based on measurement of the payloads, i.e., the active pharmaceutical ingredients. We are still blind to the exact *in vivo* fate of nanovehicles *per se* to date. Discrimination of the *in vivo* behaviors of integral vehicles from free drugs helps to justify the contribution of the nanocarriers to overall efficacy or toxicity and thereby provokes incentives to optimize the delivery

Received: July 29, 2016
Revised: September 14, 2016
Accepted: October 19, 2016
Published: October 19, 2016

DOI: 10.1021/acs.molpharmaceut.6b00705
Mol. Pharmaceutics 2016, 13, 4013–4019

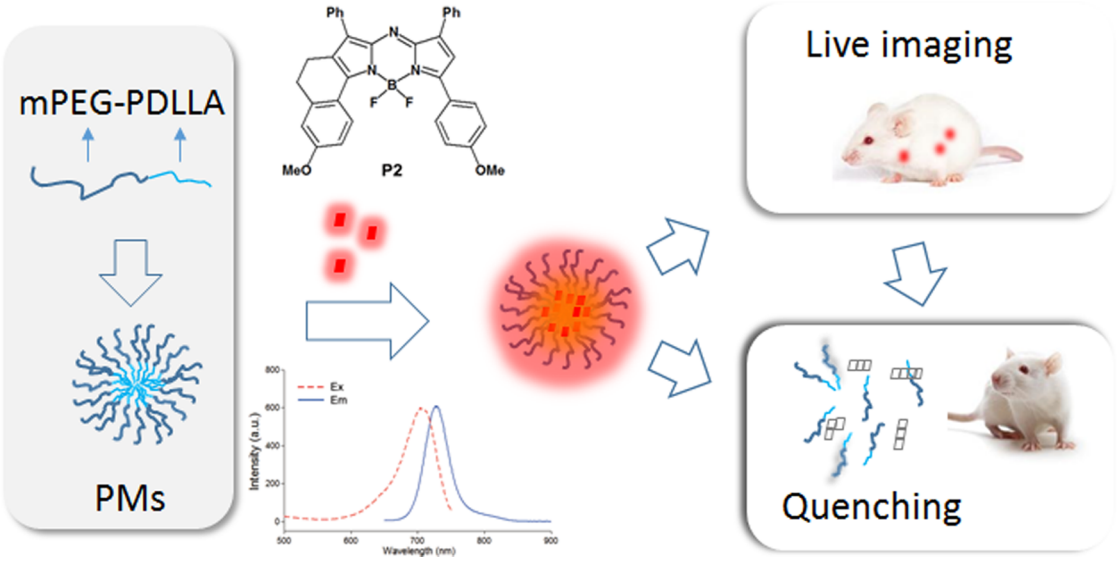

Figure 1. Rationale of the formation of mPEG−PDLLA polymeric micelles (PMs) and labeling by a water-quenching near-infrared fluorescent dye P2 for *in vivo* live imaging.

systems and expedite the whole development process. Herein, we employ a facile and accurate strategy to visualize the *in vivo* fate of integral methoxy PEG (mPEG)-poly(D,L-lactide) (PDLLA) PMs. Figure 1 is a schematic sketch of the rationale of the strategy employed in this study. In order to perform live imaging to visualize the *in vivo* fate of nanocarriers, PMs are labeled with a water-quenching environment-responsive fluorescent dye. This kind of dyes bears a parent structure of 4,4′-difluoro-4-bora-3a,4a-diaza-*s*-indacene (BODIPY) or aza-BODIPY, is highly hydrophobic, and shows nice physicochemical properties suitable for live imaging such as chemical stability, high quantum yields, and fluorescent emission in the near-infrared range. The distinct feature of this fluorescent probe rests with its ability to emit fluorescence in a well-dispersed state in hydrophobic domains, e.g., in the cores of PMs, and quenches immediately and absolutely upon release from the vehicles owing to structural disruption based on the aggregation-caused quenching (ACQ) effect.[15,16] Therefore, the recorded signals represents the signals of integral nanovehicles and can be accurately employed to interpret the *in vivo* behaviors. In favor of translation of the findings of this study into clinical use, we chose a diblock $mPEG_{2.5k}$−$PDLLA_{2.5k}$ copolymer with chain lengths similar to Genexol.

EXPERIMENTAL SECTION

Materials. Near-infrared aza-BODIPY fluorescent probe P2 was synthesized in our lab according to previous procedures.[17,18] $mPEG_{2.5k}$−$PDLLA_{2.5k}$ was synthesized by ring-opening polymerization of D,L-lactide in the presence of monopoly(ethylene glycol)[19] and kindly provided by Prof. Zhiyong Qian at Sichuan University. Ultrapure deionized water was prepared by a Milli-Q purification system (Millipore, Molsheim, France). Chloral hydrate was purchased from Sinopharm Chemical Reagent Co., Ltd. (Shanghai, China). Isoflurane was purchased from RWD Life Science Co., Ltd. (Shandong Keyuan Pharmaceutical Co., Ltd., China). SD rats (male, 150−180 g) were purchased from Shanghai Slac Laboratory Animal Co., Ltd. (Shanghai, China).

Preparation and Characterization of PMs. P2-encapsulated mPEG−PDLLA PMs were prepared using a thin-film dispersion method.[20] Briefly, mPEG−PDLLA (100 mg) and P2 (100 μg) were first dissolved in 10 mL of acetonitrile, and then the solution was evaporated under vacuum at 60 °C to form a homogeneous film in the inner wall of a flask. The obtained film was dispersed in 20 mL of deionized water under mild stirring (500 rpm) at 60 °C for 1 h. The dispersion was filtered through a 0.45 μm filter to obtain a clear and homogeneous micellar solution.

Water-quenched P2 solution was prepared and used as a control to evaluate possible interference with quantification due to rekindling of fluorescence. Briefly, 100 μg of P2 was dissolved in 100 μL of dimethyl sulfoxide (DMSO) and then diluted by water to a volume of 20 mL. The solution was stored at 4 °C for further experiments.

The average particle size, size distribution, and zeta potential of PMs were determined by dynamic light scattering (DLS) using Zetasizer Nano (Malvern Instruments, Malvern, UK) equipped with a 4 mW He−Ne laser at 633 nm under ambient temperature. All measurements were performed with a scattering angle of 173° at 25 °C after diluting the micellar solution to an appropriate volume with deionized water. JEM-1230 transmission electron microscope (TEM) (JEOL, Tokyo, Japan) was employed to study the morphology of PMs after staining with 1% phosphotungstic acid.

Determination of Critical Micelle Concentration (CMC). The CMC of mPEG−PDLLA was measured as previously reported with minor modifications by monitoring pyrene emission spectra.[21,22] Briefly, various concentrations of the copolymer from 0.001 to 100 mg/L containing 2 μM pyrene were prepared and then incubated at 37 °C overnight under mild shaking. The fluorescent intensity of samples was obtained by a fluorospectrophotometer with the excitation wavelength fixed at 372 nm, while the emission wavelengths were set to 333 and 339 nm, respectively. CMC was determined from the transition point in the plot of fluorescent intensity ratio, I_{339}/I_{333}, versus the logarithm of the block copolymer concentration.

Fluorescent Stability of PMs. The stability of PMs in water and plasma was assessed by measuring the fluorescent intensity of P2-encapsulated PMs. In brief, 1 mL of P2-

DOI: 10.1021/acs.molpharmaceut.6b00705
Mol. Pharmaceutics 2016, 13, 4013−4019

encapsulated PMs was added into 19 mL of plasma and incubated at 37 °C under shaking at 100 rpm. Samples were withdrawn at time intervals after incubation, and the fluorescent intensity of samples was immediately measured by Cary Eclipse fluorospectrophotometer (Agilent, USA). In parallel, the fluorescent stability of PMs solution diluted by the same volume of ultrapure water was also evaluated.

Pharmacokinetics in Blood. To determine the pharmacokinetics, P2-encapsulated PMs (5 mg, 30 μg P2 equiv/kg, 1 mL) and quenched P2 solution of the same strength were intravenously injected into rats through the tail vein, respectively. Blood samples (200 μL) were collected from the eye socket at various time points after injection. The fluorescent intensity of blood samples was measured by IVIS Spectrum Live Imaging System (PerkinElmer, USA). Pharmacokinetic analysis was performed using DAS 2.1.1 software (State Food and Drug Administration of China).

***In Vivo* Live Imaging.** All animals were fasted overnight but allowed free access to water before experiment. Images were captured by IVIS spectrum live imaging system with excitation/emission wavelengths set to 710/760 nm.[15,16] Blank photos were taken before administration, then P2-labeled PMs and quenched P2 solution, both at a dose of 30 μg P2 equiv/kg (1 mL), were intravenously injected into rats through the tail vein, respectively. Images were taken at various time points after anesthetization using isoflurane. Guidelines on animal welfare during experiments issued by Institutional Animal Care and Use Committee at School of Pharmacy, Fudan University were strictly followed. In order to reduce artifacts owing to contamination by urine or faeces, metabolic cages were used to raise the animals throughout the whole experiment.

***Ex Vivo* Imaging.** Under the same experimental conditions as *in vivo* imaging study, P2-labeled PMs and quenched P2 solution were given to SD rats via intravenous injection through the tail vein. At different time points, the rats were anesthetized using 10% chloral hydrate solution, and cardiac perfusion was conducted using saline before sacrificing the rats to reduce the influence of blood. Various organs and tissues were collected and observed by IVIS spectrum live imaging system. Quantification was carried out by measuring either the total fluorescence of regions of interest (ROI) or average radiant efficiency (ARE). ROI stands for the total amount of PMs available, whereas ARE stands for the concentration of PMs in a definite organ or tissue.

RESULTS

The diblock copolymer mPEG−PDLLA used in this study has similar chain lengths of both $mPEG_{2.5k}$ and $PDLLA_{2.5k}$ to Genexol.[23] The particle size of PMs prepared in this study is 30.96 ± 0.787 nm (Figure 2B), which is also similar to Genexol, with monodisperse size distribution (PDI = 0.084 ± 0.008) and slightly negative zeta potential (ζ = −3.78 ± 0.336 mV). TEM shows spherical PMs in well-dispersed state (Figure 2A). The fluorescence of P2-labeled PMs remains at ±5% of original intensity in water, indicating excellent stability and negligible leakage of the dyes over a period of 48 h (Figure 2C). However, the kinetics in plasma differs from that in water significantly with total fluorescence intensity decreasing gradually to approximately 85% and 65% at 24 and 48 h, respectively (Figure 2C). The CMC of the copolymer $mPEG_{2.5k}$-$PDLLA_{2.5k}$ is 2.93 μg/mL as determined by monitoring the pyrene emission spectra (Figure 1S).

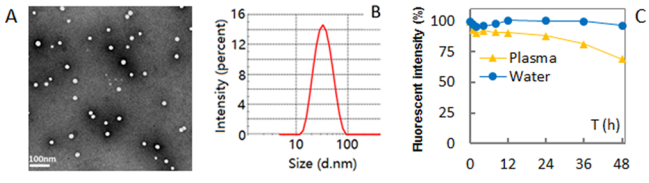

Figure 2. TEM photograph (A), particle size distribution (B), and fluorescent stability of mPEG−PDLLA polymeric micelles in either water or plasma (C).

Following intravenous injection, the pharmacokinetics of P2-labeled PMs in the systemic circulation are investigated by measuring blood-borne fluorescence. Very good linearity is established between total fluorescent intensity (Y) and the concentration of PMs (C, μg/mL) in the range of 9.77−625 μg/mL: $Y = 2.438 \times 10^6 C + 2.112 \times 10^6$, $R^2 = 0.9998$. Therefore, the fluorescent intensity observed can be used to represent the concentration of PMs in blood. In order to highlight the degree of concentration variation, the concentration at each time point of the pharmacokinetic profile is presented as percentages of the first measurement at 5 min. This presentation highlights the degree of concentration changes but does not alter the main pharmacokinetic parameters. The fluorescence intensity shows a visually decreasing tendency (Figure 3A), and quantification by ARE

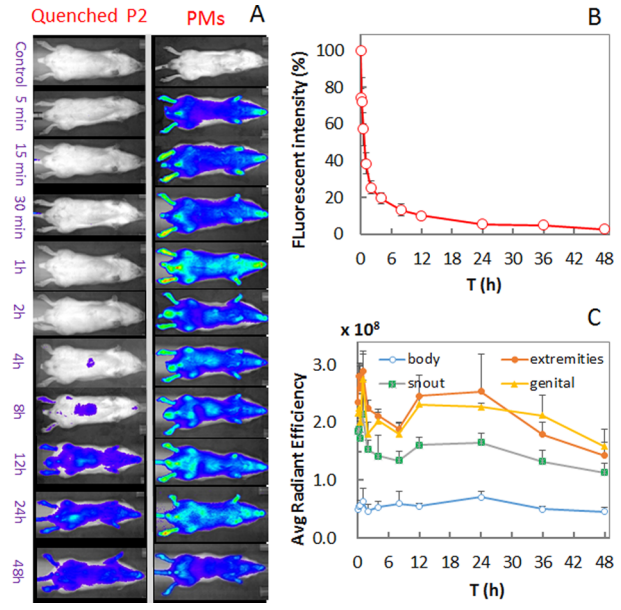

Figure 3. Live imaging of P2-labeled PMs after i.v. administration to rats (A), plasma pharmacokinetic profile (B), and fractionized quantification of fluorescence of regions of interest as average radiant efficiency [p/s/cm²/sr]/[μW/cm²] (C).

gives a pharmacokinetic profile that can be graciously fitted to a tricompartmental model (Figure 3B). The pharmacokinetic parameters $t_{1/2\alpha}$, $t_{1/2\beta}$, and $t_{1/2\gamma}$ are 0.413, 3.371, and 24.506 h, whereas K_{10}, K_{12}, K_{21}, K_{13}, and K_{31} are 0.172, 0.764, 0.679, 0.21, and 0.086 h^{-1}, respectively.

In vivo live imaging reveals pervasive distribution of PMs throughout the body for as long as 48 h. The most significant feature of biodistribution is the apparent distribution of PMs to the regions of four extremities, snout, and genitals (Figure 3A). A rough estimation of ARE, used to represent the

DOI: 10.1021/acs.molpharmaceut.6b00705
Mol. Pharmaceutics 2016, 13, 4013−4019

concentration of PMs, confirms significantly augmented accumulation of PMs to extremital tissues in the order of four extremities > snout > genital > trunk (Figure 3B). Double peaks can be found in the biodistribution plots of four extremities, snout, and genitals. The fluorescence intensity first peaks at around 1 h and subsides quickly afterward. After 8 h, there is a parallel resurgence of fluorescence in all tissues observed. To the end of 48 h, relatively high levels of fluorescence can still be observed. The control group of quenched P2 dye shows faint but incremental fluorescence after 4 h (Figure 3A, Figure 2S). It is easily understandable that after an initial phase of distribution to the tissues the dyes are able to accumulate in various tissues, where abundant lipids or surfactants are available, and be rekindled due to facilitated solubilization of the dyes in the lipid domains.

After sacrificing the animals, the biodistribution of PMs into various organs or tissues is monitored using IVIS live imaging systems (Figure 4A). After 30 min, PMs begin to accumulate in various RES organs including liver, spleen, lung, and kidney, as well as heart, adrenal glands, mesenteries, pancreas, bone marrow, and several peripheral organs or tissues such as testicles and skin. The most notable accumulation is with the vital organs, i.e., liver, spleen, and lung. It is of note that brain is the only organ observed that does not show any signal of PMs at all time points. Quantification of fluorescence reveals a trend of biodistribution to vital organs in an order of lung > liver > spleen > heart > kidney in average radiant efficiency (Figure 4B–D), but an order of liver > lung > spleen > heart ≈ kidney in total amount. The control group of quenched P2 dye also shows faint reillumination of fluorescence in some of the organs or tissues (Figure 4A, Figure 3S).

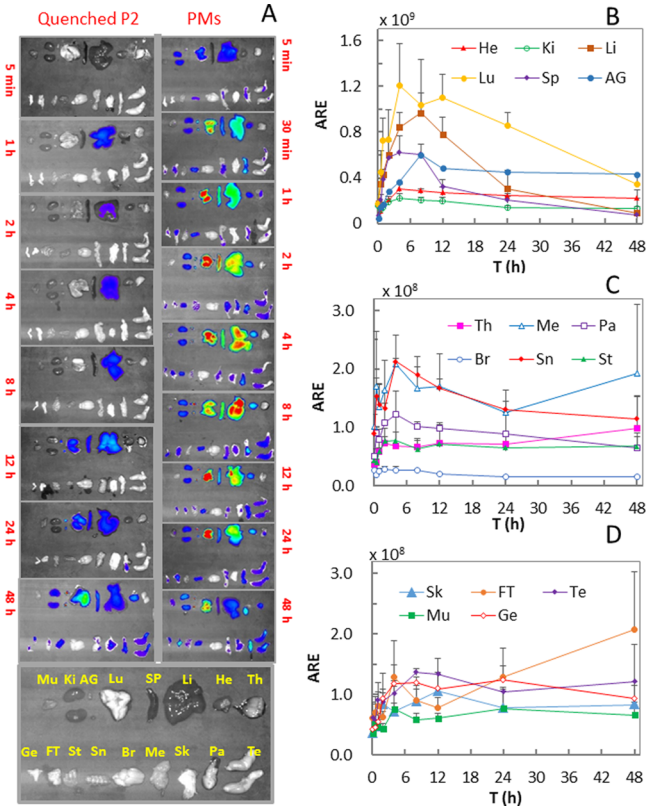

Figure 4. Live imaging of *ex vivo* organs and tissues after i.v. administration of P2-labeled PMs (A), and fluorescent intensity versus time profiles of various organs and tissues (B–D). Abbreviations: ARE, Average Radiant Efficiency [(p/s/cm^2/sr)/(μW/cm^2)]; Li (liver), Lu (lung), He (heart), K_i (kidney), AG (adrenal gland), Br (brain), Pa (pancreas), Sn (spine), Th (thymus), St (sternum), Me (mesentery), Sk (skin), FT (fatty tissue), Te (testicles), Mu (muscle), Ge (genital).

DISCUSSION

The reliability of the interpretation of *in vivo* fate of PMs depends highly on the strategies taken to identify PMs as integral vehicles. Therefore, the reliability of fluorescent labeling by water-quenching P2 dye is investigated first. In our previous work,[15,16] the water-quenching dyes have been successfully used to label solid lipid nanoparticles (SLNs). Since PMs are very small in size and do not possess sufficient space to encapsulate large amount of dyes, the encapsulation efficiency of P2 in PMs (70–80%) is not as high as in SLNs (>90%). Excessive P2 dyes that cannot be retained in the hydrophobic cores of PMs readily dissipate into the aqueous phase during preparation. Due to the ACQ effect,[24,25] unencapsulated dyes will remain in an inactivated state and do not emit fluorescence. Once PMs are formed and a balance is reached, the fluorescence of the PMs stays stable for over 48 h with less than 5% loss of total fluorescence. The time-dependent stability strongly supports the feasibility of labeling PMs with the water-quenching dyes and sets the basis for identifying integral PMs by monitoring P2 fluorescence. When being incubated with plasma, the total fluorescence shows some degree of attenuation, indicating partial dissociation of the PMs vehicles. This phenomenon does not mean that there is outward diffusion of the dyes, which might compromise the accuracy of the measurement of PMs. On the contrary, the kinetics of fluorescence quenching in plasma simulate the virtual process in the bloodstream, suggesting partial dissociation of PMs. In spite of this, the residual of about 85% and 65% fluorescence at days 1 and 2, respectively, indicates that PMs might possess certain robustness to withstand unpredictable factors in the body and keep relative integrity.

Another even more important aspect of the strategy taken in this study is the accuracy of measurement. From previous experience, quantification or even semiquantification is hardly reliable owing to the significant interference associated with fluorescence-based imaging. However, we manage to carry out a rough estimation based on the dose dependency of fluorescence within a certain range. The water-quenching probes differ from conventional fluorescent probes because they follow an on → off signal transition mode, which greatly improves the accuracy of signal judgment. It is proposed that the disappearance of the signals would unequivocally confirm the disruption of the integral vehicles.[15,16] However, one of the limitations of this kind of probes is that free or released dye molecules may be reactivated under certain circumstances by forming micelles with surfactants. Therefore, the interference of quenched free dyes was evaluated following similar administration protocols. Live imaging indicates that quenched P2 aqueous solution begins to show faint fluorescence at 4 h after injection, which strengthens over time (Figure 3A, Figure 2S). Similarly, *ex vivo* samples of organs, tissues, or blood also show some degree of reactivation of the dyes, though faintly (Figure 4A, Figure 3S). Seemingly, the rekindling of quenched free dyes may impose some degree of interference to blur the judgment of the results. However, it should be noted that the observed reillumination of fluorescence in this study stands for the

DOI: 10.1021/acs.molpharmaceut.6b00705
Mol. Pharmaceutics 2016, 13, 4013–4019

maximum interference, which can only be observed in cases when the vehicles are completely disrupted and the dyes are released instantaneously upon administration. In fact, this hardly happens because the nanovehicles for biomedicines are commonly designed to achieve sustained release or no release at all during transportation in the circulation. It is logical to reason that the less the dyes released, the less the interference caused by reillumination. As indicated by the robustness of fluorescent stability (Figure 2), there is little release of P2 to as long as 48 h in water due to the high hydrophobicity of the dye. Considering the fluorescent stability of PMs in blood, there is only 15% and 35% decrease in fluorescence at 24 and 48 h. Therefore, it is concluded that possible interference on PM detection due to reillumination might be very low and will not impose significant influence on the judgment of the results.

Another concern over the accuracy of measurement of PMs is with possible artifacts due to contamination by urine or faeces. First of all, both urine and faeces are scrutinized for any trace of P2-derived fluorescence, and results show no P2 signals at all. In spite of this, metabolic cages are used throughout the experiment to avoid any possible contamination due to urine or faeces.

The pharmacokinetic parameters reveal some fundamental information on the disposition of PMs in the circulation. The general elimination of PMs from the central compartment (CC) is very quick with a $t_{1/2\alpha}$ less than half an hour. Elimination from the first peripheral compartment (PC_1) is moderately prolonged with $t_{1/2\beta}$ of 3.371 h, whereas elimination from the second peripheral compartment (PC_2) is significantly elongated with a $t_{1/2\gamma}$ of 24.506 h. In fact, the very quick elimination rate of PMs from the CC represents a sum of three elimination rates, i.e., $K_{10} + K_{12} + K_{13}$. Since both K_{10} and K_{13} are not high enough, the K_{12} contributes the most to the overall elimination rate. Although the various compartments are conceptual, there is some correlation in the characteristics between pharmacokinetics and biodistribution. Apparently, the slow elimination rate from PC_2 (K_{31}) correlates with the sustained accumulation of PMs to peripheral tissues (Figure 3). A moderate elimination (K_{21}) can be explained by the gradual decreasing trend in the RES organs. Seemingly, CC, PC_1, and PC_2 correlate closely to physical compartments, i.e., blood tank, RES organs, and peripheral tissues, respectively. However, we should be aware of the limitations of the conventional pharmacokinetic model that elimination occurs through the CC, which is obviously not correct because PMs are probably degraded in both RES organs and peripheral tissues, and not all PMs will be eliminated via the circulation. If the findings with $mPEG_{2.5k}$−$PDLLA_{2.5k}$ PMs in this study are transplanted to the commercial product Genexol, it is suggested that the PM vehicles of Genexol will be cleared from blood quickly, accumulate in RES organs and distribute into peripheral tissues and be retained there for extended duration. Since the payload of Genexol, paclitaxel, is highly hydrophobic and does not leak from the vehicles very quickly, the exposure time and dosage of the toxic drug at the vital organs and peripheral tissues are significant, and their effects on the toxicological profiles of this product should not be ignored.

After injection, PMs distribute spontaneously throughout the whole body and gradually accumulate in four extremities, snouts, and the genitals with fluorescent intensity 3−5 times higher than the body area. Although there is no clear interpretation to this phenomenon yet, we believe the relatively low temperature of these tissues may create more resistance to the transport of the nanoparticles and thus trap the PMs. This finding reminds us that if the nanocarriers are loaded with toxins such as in the case of chemotherapy, the toxins tend to be released and accumulate in these tissues, resulting in local toxicity. Clinical phase I trials indicate that neuropathy and myalgia are the most common toxicities of Genexol−PM,[26,27] while phase II trials further revealed the common toxicities of anemia, asthenia, myalgia, peripheral neuropathy, and diarrhea with occurrence of 30−70%.[13] It is reasonable to propose that there might be some relationship between the biodistribution of PMs and their observed peripheral toxicities. However, the finding here may be extrapolated to explain the peripheral toxicity of marketed long-circulating delivery system, e.g., the PEGylated doxorubicin liposomes.[28−30] Namely, hand-and-foot syndrome and peripheral neuropathy are probably due to the enhanced accumulation of the vehicles to these peripheral tissues.

Body distribution reveals more important characteristics of translocation of PMs. Though being coated with a layer of PEG chains, it is not efficient enough to camouflage the vehicles from being recognized by the mechanisms of opsonization and phagocytosis. Most of the PMs are found distributing to macrophage-enriched organs, i.e., the vital organs such as lung, liver, spleen, and kidney with intensity a few to ten times higher than to other organs or tissues. Noticeably, there is no distribution to the brain at all, which means that it is not enough to enhance transportation across the blood−brain barrier (BBB) by simply prolonging the circulating time, which however contradicts previous findings that stealth nanoparticles significantly enhances trans-BBB transportation.[31,32] It should also be noted that our findings here only prove that there is no permeation of PMs into the brain, but there is still possibility that the encapsulated drug molecules can be transported in more amount owing to the long-circulating effect. Based on the above findings, it is rational to conclude that although PEGylation significantly reduces the toxicity of free drugs, the vital organs are still vulnerable to the harmful effect due to specific accumulation of PMs.

By comparing the biodistribution profiles of peripheral tissues to vital organs, interesting conclusions on the mechanisms of biodistribution can be inferred. As shown in Figure 3C, the first peak of distribution at around 1 h might be due to the fast perfusion of PMs into the peripheral tissues. After the first peak, distribution of PMs at these tissues decrease gradually and valleyed at around 4−6 h (Figure 3C), which nevertheless coincides with the peaking in various vital organs, especially liver (Figure 4B−D). Apparently, the decrease of peripheral distribution can be attributed to the recognition and uptake of PMs by these RES organs. The second prolonged and mild resurgence of fluorescence in peripheral tissues at around 8−24 h (Figure 3C) implies that there is a reperfusion of the particles into the peripheral tissues. Then, what is the source of PMs for the second resurgence in peripheral tissues? The most confirmative answer might be the vital organs because there is apparent accumulation of PMs in these organs, almost an order higher than other organs or tissues, and corresponding decrease after 8 h (Figure 4B). An explanation of release from the RES organs and subsequent translocation of PMs to the periphery tissues sounds reasonable.

Unlike nanoparticles with a polymer matrix, PMs are self-assemblies that are held together by hydrophobic driving forces. CMC plays a crucial role in determining the stability or integrity of polymeric micelles. At concentrations below CMC,

DOI: 10.1021/acs.molpharmaceut.6b00705
Mol. Pharmaceutics 2016, 13, 4013−4019

PMs are supposed to dissociate quickly and divulge the payloads. If we take the total blood volume of a rat as 10 mL, the calculated blood concentration of PMs here would be 500 μg/mL (5 mg/10 mL). The reported CMC for Genexol is 7 μg/mL[33] and for PEG_{2k}−$PDLLA_{2k}$ PMs it is 3.16 μg/mL.[34] The measured value for the PMs ($mPEG_{2.5k}$−$PDLLA_{2.5k}$) in this study is 2.93 μg/mL, similar to reports on PMs of similar chain lengths. In general, the calculated mPEG−PDLLA PMs concentration of about 500 μg/mL *in vivo* is significantly higher than the CMC measured. Therefore, there is no worry about dissociation of PMs due to dilution *in vivo*.

Since PMs are new in the market, there are still limited data on its pharmacological and toxicological effects. The study presents useful information to remind physicians of the potential harm of this product. There is good chance to translate these results into clinical use.

CONCLUSIONS

In vitro fluorescent stability and water-quenching study confirms the feasibility of using a novel water-quenching P2 dye to label and identify integral vehicles of PMs. Live imaging in rats indicates specific distribution of PMs to the extremities with 3−5 times higher concentration. *Ex vivo* examination shows accumulated distribution to vital organs such as the lung, liver, spleen, and kidney. It is concluded that long-circulating decoration helps to divert a fraction of PMs to peripheral tissues, but a large fraction of PMs are still captured by the macrophage-rich organs. Therefore, the specific distribution of PMs to extremities and vital organs warns of potential toxicity if a toxin is encapsulated.

ASSOCIATED CONTENT

Supporting Information

The Supporting Information is available free of charge on the ACS Publications website at DOI: 10.1021/acs.molpharmaceut.6b00705.

CMC determination plot of mPEG2.5k−PDLLA2.5k copolymer, live imaging of reillumination of quenched P2 dye, and ex vivo imaging of reillumination of quenched P2 dye (PDF)

AUTHOR INFORMATION

Corresponding Authors

*Tel/fax: +862151980084. E-mail: wuwei@shmu.edu.cn.
*Tel/fax: +862151980084. E-mail: zhaoweili@fudan.edu.cn.

Author Contributions

§H.H. and J.Z. contributed equally to this article.

Notes

The authors declare no competing financial interest.

ACKNOWLEDGMENTS

This study was financially supported by National Natural Science Foundation of China (81573363, 21372063), Shanghai Commission of Science and Technology (14JC1490300).

REFERENCES

(1) Amoozgar, Z.; Yeo, Y. Recent Advances in Stealth Coating of Nanoparticle Drug Delivery Systems. *Wiley Interdiscip. Rev. Nanomed. Nanobiotechnol.* **2012**, *4*, 219−233.

(2) Moghimi, S. M.; Hunter, A. C.; Murray, J. C. Long-Circulating and Target-Specific Nanoparticles: Theory to Practice. *Pharmacol. Rev.* **2001**, *53*, 283−318.

(3) Maeda, H. Macromolecular Therapeutics in Cancer Treatment: the EPR Effect and beyond. *J. Controlled Release* **2012**, *164*, 138−144.

(4) Nichols, J. W.; Bae, Y. H. EPR: Evidence and Fallacy. *J. Controlled Release* **2014**, *190*, 451−464.

(5) Barenholz, Y. Doxil®-the First FDA-Approved Nano-Drug: Lessons Learned. *J. Controlled Release* **2012**, *160*, 117−134.

(6) Duggan, S. T.; Keating, G. M. Pegylated Liposomal Doxorubicin: a Review of Its Use in Metastatic Breast Cancer, Ovarian Cancer, Multiple Myeloma and AIDS-Related Kaposi's Sarcoma. *Drugs* **2011**, *71*, 2531−2558.

(7) Wang, C.; Wang, Y.; Wang, Y.; Fan, M.; Luo, F.; Qian, Z. Characterization, Pharmacokinetics and Disposition of Novel Nano-scale Preparations of Paclitaxel. *Int. J. Pharm.* **2011**, *414*, 251−259.

(8) Gao, X.; Wang, B.; Wu, Q.; Wei, X.; Zheng, F.; Men, K.; Shi, H.; Huang, N.; Wei, Y.; Gong, C. Combined Delivery and Anti-Cancer Activity of Paclitaxel and Curcumin Using Polymeric Micelles. *J. Biomed. Nanotechnol.* **2015**, *11*, 578−589.

(9) Cho, H.; Lai, T. C.; Tomoda, K.; Kwon, G. S. Polymeric Micellesfor Multi-Drug Delivery in Cancer. *AAPS PharmSciTech* **2015**, *16*, 10−20.

(10) Li, H.; Li, X.; Zhang, C.; Sun, Q.; Yi, W.; Wang, X.; Cheng, D.; Chen, S.; Liang, B.; Shuai, X. Regulated pH-Responsive Polymeric Micelles for Doxorubicin Delivery to the Nucleus of Liver Cancer Cells. *J. Biomed. Nanotechnol.* **2016**, *12*, 1258−1269.

(11) Yang, H. Y.; Jang, M. S.; Gao, G. H.; Lee, J. H.; Lee, D. S. pH-Responsive Biodegradable Polymeric Micelleswith Anchors to Interface Magnetic Nanoparticles for MR Imaging in Detection of Cerebral Ischemic Area. *Nanoscale* **2016**, *8*, 12588−12598.

(12) Zhao, L.; Yang, C.; Dou, J.; Xi, Y.; Lou, H.; Zhai, G. Development of RGD-Functionalized PEG-PLA Micelles for Delivery of Curcumin. *J. Biomed. Nanotechnol.* **2015**, *11*, 436−446.

(13) Ahn, H. K.; Jung, M.; Sym, S. J.; Shin, D. B.; Kang, S. M.; Kyung, S. Y.; Park, J. W.; Jeong, S. H.; Cho, E. K. A Phase II Trial of Cremorphor EL-Free Paclitaxel(Genexol-PM) and Gemcitabine in Patients with Advanced Non-Small Cell Lung Cancer. *Cancer Chemother. Pharmacol.* **2014**, *74*, 277−282.

(14) Cabral, H.; Kataoka, K. Progress of Drug-Loaded Polymeric Micelles into Clinical Studies. *J. Controlled Release* **2014**, *190*, 465−476.

(15) Hu, X.; Zhang, J.; Yu, Z.; Xie, Y.; He, H.; Qi, J.; Dong, X. C.; Lu, Y.; Zhao, W. L.; Wu, W. Environment-Responsive Aza-BODIPY Dyes Quenching in Water as Potential Probes to Visualize the in Vivo Fate of Lipid-based Nanocarriers. *Nanomedicine* **2015**, *11*, 1939−1948.

(16) Hu, X.; Fan, W.; Yu, Z.; Lu, Y.; Qi, J.; Zhang, J.; Dong, X. C.; Zhao, W. L.; Wu, W. Evidence Does not Support Absorption of Intact Solid Lipid Nanoparticles via Oral Delivery. *Nanoscale* **2016**, *8*, 7024−7035.

(17) Zhao, W. L.; Carreira, E. M. Conformationally Restricted Aza-Bodipy: a Highly Fluorescent, Stable, Near-Infrared-Absorbing Dye. *Angew. Chem., Int. Ed.* **2005**, *44*, 1677−1679.

(18) Zhao, W. L.; Carreira, E. M. Conformationally Restricted Aza-BODIPY: Highly Fluorescent, Stable Near-Infrared Absorbing Dyes. *Chem. - Eur. J.* **2006**, *12*, 7254−7263.

(19) Zheng, X.; Kan, B.; Gou, M.; Fu, S.; Zhang, J.; Men, K.; Chen, L.; Luo, F.; Zhao, Y.; Zhao, X.; Wei, Y.; Qian, Z. Preparation of MPEG-PLA Nanoparticle for Honokiol Delivery in Vitro. *Int. J. Pharm.* **2010**, *386*, 262−267.

(20) Wang, Y.; Wang, C.; Wang, Y.; Luo, F.; Yan, X.; Qian, Z. Micelles of Methoxy Poly(ethylene glycol)-poly(epsilon-caprolactone) as a Novel Drug Delivery Vehicle for Tacrolimus. *J. Biomed. Nanotechnol.* **2013**, *9*, 147−157.

(21) Nagasaki, Y.; Okada, T.; Scholz, C.; Iijima, M.; Kato, M.; Kataoka, K. The Reactive Polymeric Micelle Based on An Aldehyde-Ended Poly(ethylene glycol)/Poly(lactide) Block Copolymer. *Macromolecules* **1998**, *31*, 1473−1479.

(22) Lee, S. C.; Huh, K. M.; Lee, J.; Cho, Y. W.; Galinsky, R. E.; Park, K. Hydrotropic Polymeric Micelles for Enhanced Paclitaxel Solubility: In Vitro and In Vivo Characterization. *Biomacromolecules* **2007**, *8*, 202−208.

DOI: 10.1021/acs.molpharmaceut.6b00705
Mol. Pharmaceutics 2016, 13, 4013−4019

(23) Kim, S. C.; Kim, D. W.; Shim, Y. H.; Bang, J. S.; Oh, H. S.; Wan Kim, S.; Seo, M. H. In Vivo Evaluation of Polymeric Micellar Paclitaxel Formulation: Toxicity and Efficacy. *J. Controlled Release* **2001**, *72*, 191−202.
(24) Birks, J. B. *Photophysics of Aromatic Molecules*; Wiley: London, 1970.
(25) Jenekhe, S. A.; Osaheni, J. A. Excimers and Exciplexes of Conjugated Polymers. *Science* **1994**, *265*, 765−768.
(26) Kim, T. Y.; Kim, D. W.; Chung, J. Y.; Shin, S. G.; Kim, S. C.; Heo, D. S.; Kim, N. K.; Bang, Y. J. Phase I and Pharmacokinetic Study of Genexol-PM, a Cremophor-Free, Polymeric Micelle-Formulated Paclitaxel, in Patients with Advanced Malignancies. *Clin. Cancer Res.* **2004**, *10*, 3708−3716.
(27) Lv, F.; Cao, J.; Zhang, J.; Qian, J.; Peng, W.; Sun, S.; Li, W.; Zhang, W.; Guo, W.; Li, J. Phase I and Pharmacokinetic Study of Polymeric Micelle-Formulated Paclitaxel in Adult Chinese Patients with Advanced Solid Tumors. *Cancer Chemother. Pharmacol.* **2014**, *73*, 1173−1179.
(28) Lao, J.; Madani, J.; Puértolas, T.; Alvarez, M.; Hernández, A.; Pazo-Cid, R.; Artal, A.; Antón Torres, A. Liposomal Doxorubicin in the Treatment of Breast Cancer Patients: a Review. *J. Drug Delivery* **2013**, *2013*, 456409.
(29) von Moos, R.; Thuerlimann, B. J.; Aapro, M.; Rayson, D.; Harrold, K.; Sehouli, J.; Scotte, F.; Lorusso, D.; Dummer, R.; Lacouture, M. E.; Lademann, J.; Hauschild, A. Pegylated Liposomal Doxorubicin-Associated Hand-Foot Syndrome: Recommendations of an International Panel of Experts. *Eur. J. Cancer* **2008**, *44*, 781−790.
(30) Solomon, R.; Gabizon, A. A. Clinical Pharmacology of Liposomal Anthracyclines: Focus on Pegylated Liposomal Doxorubicin. *Clin. Lymphoma Myeloma* **2008**, *8*, 21−32.
(31) Brigger, I.; Morizet, J.; Aubert, G.; Chacun, H.; Terrier-Lacombe, M. J.; Couvreur, P.; Vassal, G. Poly(ethylene glycol)-Coated Hexadecylcyanoacrylate Nanospheres Display a Combined Effect for Brain Tumor Targeting. *J. Pharmacol. Exp. Ther.* **2002**, *303*, 928−936.
(32) Sun, W.; Xie, C.; Wang, H.; Hu, Y. Specific Role of Polysorbate 80 Coating on the Targeting of Nanoparticles to the Brain. *Biomaterials* **2004**, *25*, 3065−3071.
(33) Kim, S. C.; Yoon, H. J.; Lee, J. W.; Yu, J. Y.; Park, E. S.; Chi, S. C. Investigation of the Release Behavior of DEHP from Infusion Sets by Paclitaxel-Loaded Polymeric Micelles. *Int. J. Pharm.* **2005**, *293*, 303−310.
(34) Daman, Z.; Ostad, S. N.; Amini, M.; Gilani, K. Preparation, Optimization and In Vitro Characterization of Stearoyl-Gemcitabine Polymeric Micelles: A Comparison with its Self-Assembled Nanoparticles. *Int. J. Pharm.* **2014**, *468*, 142−151.

DOI: 10.1021/acs.molpharmaceut.6b00705
Mol. Pharmaceutics 2016, 13, 4013−4019